ACS APPLIED MATERIALS & INTERFACES

RESEARCH ARTICLE

www.acsami.org

Preparation and Characterization of PtRu Nanoparticles Supported on Nitrogen-Doped Porous Carbon for Electrooxidation of Methanol

Zhaolin Liu,*[,†] Fabing Su,[‡] Xinhui Zhang,[†] and Siok Wei Tay[†]

[†]Institute of Materials Research & Engineering, Agency for Science, Technology and Research (A*STAR), 3 Research Link, Singapore 117602,

[‡]State Key Laboratory of Multiphase Complex Systems, Institute of Process Engineering, Chinese Academy of Sciences, Beijing, China 100190

Supporting Information

ABSTRACT: N-doped porous carbon nanospheres (PCNs) were prepared by chemical activation of nonporous carbon nanospheres (CNs), which were obtained via carbonization of polypyrrole nanospheres (PNs). The catalysts, PtRu and Pt nanoparticles supported on PCNs and Vulcan XC-72 carbon black, were prepared by ethylene glycol chemical reduction. Transmission electron microscopy, X-ray diffraction, and energy-dispersive X-ray spectroscopy were employed to characterize samples. It was found that PCNs containing N function groups possess a large number of micropores. Uniform and well-dispersed Pt and PtRu particles with narrow particle size distribution were observed. The electrooxidation of liquid methanol on these catalysts was investigated at room temperature by cyclic voltammetry, chronoamperometry and electrochemical impedance spectroscopy (EIS). The results showed that alloy catalyst (Pt_1Ru_1/PCN) possessed the highest catalytic activity and better CO tolerance than the other PtRu and Pt-only catalysts; PtRu nanoparticles supported on PCN showed a higher catalytic activity and more stable sustained current than on carbon black XC-72. Compared to commercial Alfa Aesar PtRu catalyst, Pt_1Ru_1/PCN reveals an enhanced and durable catalytic activity in methanol oxidation because of the high dispersion of small PtRu nanoparticles and the presence of N species of support PCNs.

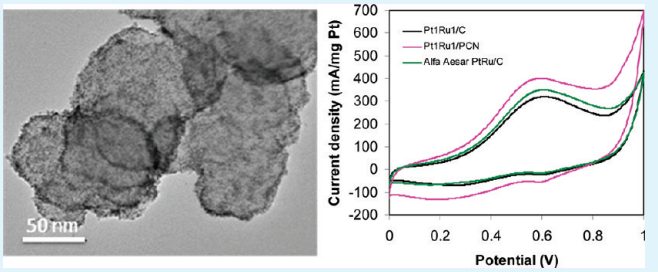

KEYWORDS: nitrogen-doped porous carbon, catalyst, methanol oxidation, fuel cell

INTRODUCTION

Direct methanol fuel cells (DMFC) are one of the potential power sources for portable electronic devices. Challenging issues such as methanol crossover, low catalytic activity of electrodes both for the oxygen reduction and for the methanol oxidation reaction, high costs of the Pt-based electrocatalysts, and susceptibility of the catalysts to be poisoned by the CO-like intermediates formed in the methanol oxidation reaction are the main obstacles to the commercialization of DMFC technology. Fundamental worldwide research efforts are currently directed towards the development of anode electrocatalysts with high catalytic activity.[1] To achieve high dispersion, utilization, activity, and stability of noble Pt and its alloys, carbon materials as supports with developed pore structure, high surface area, nanoscaled morphology, tunable surface chemistry, and good electric conductivity are highly desirable for electrocatalysts.[2−5] Yu and co-workers[6,7] reported ordered uniform porous carbon with pore sizes in the range of 10 to ∼1000 nm demonstrated its possibility as a good catalyst support in a direct methanol fuel cell. Recently, Liu and co-workers[8] have synthesized PtRu nanoparticles of ca. 2−3 nm on carbon mesoporous (PtRu-CMMs) directly using SBA-15 mesoporous silica as the template, furfuryl alcohol, and trimethylbenzene as the primary carbon source. The ordered mesoporous carbon with high surface area and regular pore channels can facilitate reactant/product diffusion. Li and co workers[9] have reported that the high surface area of the ball-milled multiwall carbon nanotubes (MWCNTs) with plenty of mesopores and defects may contribute to the high Pd−Co utility and consequently to the better electrochemical activity.

It has been proven that the presence of functional groups such as N species on the carbon support surface could lead to the high dispersion of fine Pt nanoparticles with the synergistic interaction of Pt and support, resulting in the improved catalytic activity and durability toward oxygen reduction reaction (ORR) and methanol oxidation reaction (MOR).[10] Much work focused on the N-doped carbon materials with N species incorporated in the carbon matrix to promote the Pt/carbon electrocatalyst performance. For example, Pt-based metal nanoparticles supported on carbon nitride (CN_x) materials[11−14] and N-containing mesoporous carbons[15,16] exhibited high electrocatalytic activities in

Received: February 21, 2011
Accepted: September 15, 2011
Published: September 15, 2011

MOR and/or ORR. On the other hand, pore structure including mesopores and micropores in templated carbon supports has been demonstrated to play a significant role in transferring the mass products in MOR and ORR.[17,18] Recently, Lei and co workers[19] and Choi and co-workers[20] have found that the N-doped carbon nanoparticles as Pt catalyst support was superior compared to XC-72 in MOR activity, but these carbon nanoparticles have no developed pore structure. The commercial electrocatalyst support such as carbon black XC-72 is carbon nanoparticles with a diameter of less than 100 nm. The voids among these nanoparticles could form a three-dimensional mesoporous structure that provides a rapid mass transport within electrodes. However, these particles do not contain N species. Shen and co-workers[21] have also reported that the Pt supported on carbon nanotubes (CNTs) treated by H_2O_2 solution demonstrate improved dispersion and high activity for MOR. In our previous work,[22] the electrochemical properties of Pt/PCN, Pt/CN, and Pt/PN catalysts showed that Pt/PN catalyst is inactive toward MOR and ORR at room temperature due to the high intrinsic resistance of PNs. Compared to Pt/CN, Pt/PCN revealed an enhanced performance in ORR and MOR because of the high dispersion of small Pt nanoparticles on PCNs, which possess a developed pore structure, high surface area, and N species.

In this paper, PtRu nanoparticles supported on PCNs were prepared by a simple microwave-assisted polyol procedure. We sought to use PCNs as support to prepare PtRu alloy nanoparticles; it was found for the first time that PtRu nanoparticles were successfully synthesized and captured by PCNs support material suspended in the solution. Microwave dielectric loss heating may be a better synthesis option in view of its energy efficiency, speed, uniformity, and implementation simplicity.

The physicochemical properties and electrochemical activities of electrocatalysts PtRu/PCN were comparatively examined for MOR. It was found that toward MOR, PtRu/PCN catalysts showed a better performance than commercial Alfa Aesar catalyst (20 wt % Pt, 10 wt % Ru), indicating a highly potential application of PCNs in fuel cells.

EXPERIMENTAL SECTION

Synthesis of Support Nanospheres and PtRu Catalysts. The samples PNs and CNs were prepared using a method previously reported.[23] In a typical synthesis, a mixture containing decyl alcohol (1-decanol, 99%, Aldrich) (1.0 g) and deionized water (30 mL) was stirred at 1 °C for 10 min. Then, dodecyltrimethylammonium bromide (DTAB, 99%, Aldrich) (1.5 g) was added to this mixture still under stirring at 1 °C for 20 min. The above mixture was transferred into a plastic tube. Subsequently, a 0.8 g of pyrrole (98%, Aldrich) was added dropwise into the tube, which was sonicated in an ultrasonicator. After 5 min, powdered $FeCl_3$ (99%, Aldrich) (2.0 g) was added into the tube. After further ultrasonication for 30 min, the product PNs were separated by centrifugation, washed with ethanol and water, and dried in an oven at 60 °C over night under a vacuum. The PNs were carbonized in a quartz tube at 800 °C for 2 h under a nitrogen atmosphere to obtain sample CNs. CNs were further mixed with powdered solid KOH (98%, Aldrich) at a mass ratio of 1:1 for chemical activation. The mixture was heated to 900 °C with a heating rate of 5 °C min^{-1} under a flow of nitrogen and retained for 30 min. The solid was finally washed with diluted HCl solution and distilled water to completely remove metal species, and dried at 120 °C for 4 h to obtain sample PCNs.

PtRu catalysts supported on PCNs were synthesized by the ethylene glycol (EG) reduction method.[24] The Pt content in each sample was 20 wt %. A typical preparation of Pt_3Ru_1/PCN, Pt_2Ru_1/PCN, and Pt_1Ru_1/PCN catalysts (subscript denotes the atomic ratio of the alloying metal) would consist of the following steps: In a 100 mL beaker, 2.6 mL of 0.02 M $H_2PtCl_6 \cdot 6H_2O$ and 0.87, 1.3, and 2.6 mL of 0.02 M $RuCl_3$ were mixed with 20 mL of ethylene glycol (Mallinckrodt, AR). 0.2 mL of 1 M NaOH was added dropwise. 0.040 g of PCN or Vulcan XC-72 carbon support was added to the mixture and sonicated for 30 min. The beaker and its contents were heated in a household microwave oven (National NN-S327WF, 2450 MHz, 700 W) for 50 s. The resulting suspension was filtered, and the residue was washed with acetone and dried at 60 °C overnight in a vacuum oven. The prepared PtRu catalysts supported on PCNs and Vulcan XC-72 carbon were assigned as PtRu/PCN and PtRu/C, respectively.

Characterization. The particle morphology, size, and size-distribution of the catalysts were characterized by transmission electron microscopy (TEM) using a Philips CM300 FEG system operating at 300 kV. The TEM samples were prepared by placing a drop of the sonicated (1 h) catalyst suspension in acetone on a 3 mm Cu grid, following by drying under ambient conditions. The amount of elements was determined by Oxford INCA energy-dispersive X-ray (EDX) spectrometer. Thermogravimetric analysis (TGA) was conducted on a thermogravimetric analyzer TA Q500 (Thermal Analysis Instruments, U.S.A.). X-ray diffraction (XRD) patterns were recorded by means of Bruker GADDS diffractometer with an area detector that used a Cu Kα source (λ = 1.54056 Å) operating at 40 kV and 40 mA. The XRD samples were obtained by depositing carbon-supported nanoparticles on a glass slide and then drying overnight under vacuum.

An AUTOLAB potentiostat/galvanostat and a conventional three-electrode test cell were used for electrochemical measurements. The working electrode was a thin layer of Nafion-impregnated catalyst cast on a vitreous carbon disc held in a Teflon cylinder. The catalyst layer was obtained as follows: (i) a slurry was first prepared by sonicating for 1 h a mixture of 0.5 ml of de-ionized water, 0.013 g of the catalyst, and 0.11 mL of Nafion solution (Aldrich: 5 wt.% Nafion); (ii) 4 μL of the slurry was pipetted and spread on the carbon disc; (iii) the electrode was dried at 90 °C for 1 h and mounted on a stainless-steel support. The surface area of the vitreous carbon disc was 0.25 cm^2. A Pt gauze and a Ag/AgCl electrode were used as the counter and reference electrodes, respectively. All potentials are reported with respect to the Ag/AgCl electrode. All electrolyte solutions were purged with high-purity argon for 2 h prior to each measurement. For cyclic voltammetry and chronoamperometry of methanol oxidation, the electrolyte solution was 2 M CH_3OH in 1 M H_2SO_4 and was prepared from high-purity sulfuric acid, high-purity methanol, and distilled water. Electrochemical impedance spectroscopy (EIS) of the samples was measured in 2 M CH_3OH and 1 M H_2SO_4 solution over the frequency range from 1×10^5 to 0.01 Hz at around 0.4 V. All measurements were carried out at room temperature.

RESULTS AND DISCUSSION

Physicochemical Characterization of Support and PtRu Catalysts. The TEM images of support samples PNs, CNs, and PCNs are shown in Figure S1 in the Supporting Information. The particle size of PNs is in the range of 100−150 nm in the diameter shown in Figure S1a in the Supporting Information. The EDX analysis of PNs indicates the presence of C (69 wt %), N (20 wt %), O (9 wt %), Fe (1 wt %), and Cl (1 wt %). The atomic ratio of N/C is ~0.25, consistent with that of the polypyrrole unit (−C_4NH_2−) (N/C = 0.25). CNs are relatively smaller than their parent PNs due to the shrinkage during carbonization process (see Figure S1b in the Supporting Information). The rough surface of CNs may stem from the heterogeneous

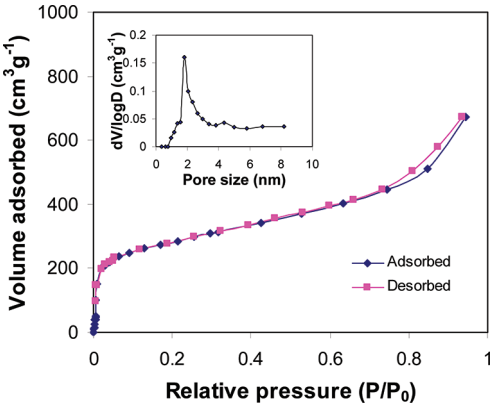

Figure 1. Nitrogen adsorption/desorption isotherms of a PCNs mesoporous carbon template, together with its pore size distribution curves (inset).

shrinkage. The mass content of C, N, O, and Fe derived from EDX analysis for sample CNs is 82, 11, 5, and 2 wt %, respectively, and no signal from Cl was detected. The atomic ration of N/C is approximate 0.12, almost half of that of the PNs, suggesting that the carbonization process would reduce the concentration of N species more quickly relative to C because the denitrogenation, dehydrogenation, and aromatization occurred. Figure S1c in the Supporting Information shows the morphology of PCNs, whose surface looks much coarser than CNs. This may result from the etching of the carbon matrix by chemical activating agent. C (89 wt %), N (4 wt %), O (5 wt %), K (1 wt %), and Fe (1 wt %) in PCNs were found using EDX. The atomic ratio of N/C is ~0.05, much less than that of CNs. This may indicate some N species within CNs are more active during chemical activation and readily gasified. The TEM image of the PCNs in Figure S1d in the Supporting Information clearly shows the microporous structure of PCNs with more exposed graphene edges as well as defects. PCNs also have much less dense molecular structure and indistinctly discrete graphene layers when compared to the image of CNs in Figure S1e in the Supporting Information. It has been known that the chemical activation using KOH is a well established method to generate highly microporous structures for various carbonaceous materials.[25−27] At a high temperature, the alkali species is reduced to metal by the carbon species, and thus the carbon framework is etched to create a large number of micropores due to the oxidation of carbon into carbonate ion. The subsequent removal of the alkali metal species by washing with acid solution may generate additional micropores. It should be mentioned that the chemical activation using KOH could introduce much oxygen functional groups and grapheme layer defects on the surface of PCNs, which are significant for deposition and immobilization of Pt nanoparticles,[28] together with formation of strong interfacial interaction between Pt and carbon surface.[22,29−31]

Nitrogen isothermal adsorption measurements were performed to determine the pore structure and the Brunauer−Emmett−Teller (BET) surface areas of the PCNs. N_2 adsorption-desorption isotherms and pore size distribution (PSD) of PCNs is presented in Figure 1. It can be seen that the adsorption isotherm of PCNs is of type I according to the IUPAC classification, indicative of microporous materials. The remarkable nitrogen uptake above the relative pressure of 0.8 is due to the capillary condensation of nitrogen in interparticulate porosity that exists among agglomerate nanospheres forming a mesoporous texture. The inset in Figure 2 shows the PSD of PCNs derived from the density functional theory (DFT) method. The pore size of PCNs is centered at around 1.8 nm. The surface area of PCNs is 1128 $m^2\ g^{-1}$. N_2 adsorption-desorption isotherms and pore size distribution (PSD) of Vulcan carbon can be found in Figure S2 (see the Supporting Information). The type I isotherm curve indicates the microporous structure of Vulcan carbon with a pore size of less than 2 nm (see the inset of Figure S2 in the Supporting Information). The surface area of Vulcan carbon is 230 $m^2\ g^{-1}$, about 5-fold lower than that of PCNs.

In our approach, PtRu nanoparticles are prepared and directly deposited on the carbon surface by microwave heating of ethylene glycol solution of Pt and Ru salts. Figure 2 is typical TEM images of the Pt/PCN, Pt_1Ru_1/PCN, Pt/C, and Pt_1Ru_1/C, as well as commercial Alfa Aesar PtRu/C catalysts. The image of Pt/PCN catalyst in images a and b in Figure 2 shows that Pt nanoparticles are homogeneously deposited on the surface of PCNs with the high dispersion, and particles size is estimated to be ~5 nm. Images c and d in Figure 2 present the image of Pt_1Ru_1/PCN catalyst, in which PtRu nanoparticles were homogeneously dispersed on the surface of PCNs and their size is ranged from 2 to 4 nm. The images of Pt_3Ru_1/PCN and Pt_2Ru_1/PCN catalysts in Figure S3 (see the Supporting Information) exhibit similar with the results of Pt_1Ru_1/PCN; uniform and well-dispersed alloy particles. However, some aggregated Pt and PtRu nanoparticles can be found in Figures 2e−j for Pt/C, PtRu/C, and Alfa Aesar PtRu/C catalysts, and the Pt and PtRu particle size are 3−5 and 2−3 nm, respectively. Studies have proven that the presence of N species as localized defects facilitates the high dispersion and immobilization of Pt particles on the carbon supports and makes the carbon surface chemically active for the enhanced interaction between Pt and the supports.[10] For instance, Yue et al. found that Pt nanoparticles were homogeneously dispersed on the N-doped CNTs compared with pristine ones.[18] Here, it is believed that for two synthesized catalysts, the N-participation in the connection of Pt and PtRu species with the support may contribute to the improvement of Pt and PtRu particles dispersion.

The TG curves in Figure S4a (Supporting Information) shows that the weight loss of Pt/PCN, Pt_1Ru_1/PCN, Pt/C, and Alfa Aesar PtRu/C takes place in the temperature ranges 320−390, 320−410, 300−400, and 415−480 °C, respectively, obviously lower than that of their supports shown in Figure S4b (Supporting Information). This is because of the introduction of Pt or PtRu nanoparticles, which could lead to the catalytic combustion of support in air. The temperature range for main weight loss of Pt/C and Alfa Aesar PtRu/C is 300−400 and 310−400 °C, respectively, much higher than that of Pt/PCN and Pt_1Ru_1/PCN possibly due to the higher surface area of PCNs than that of Vulcan carbon (~230 m^2/g) and Alfa Aesar support, which may allow more grapheme defects exposed for oxidation. The weight loss for these samples below 200 °C should result from the desorption of water vapour. Thus, the Pt or PtRu content in the catalysts can be obtained from their TG curves after subtracting the weight of adsorbed water and residue. When the weight of the anhydrous material is set to 100 wt %, the content of Pt and PtRu in Pt/PCN, Pt_1Ru_1/PCN, Pt/C, and Alfa Aesar PtRu/C is 20.2, 30.4, 20.3, and 30.5 wt %, respectively.

The XRD patterns of Pt/PCN and PtRu/PCN catalysts are shown in Figure 3. A broad diffraction peak located at around 25.5° can be seen for four samples, corresponding to [002]

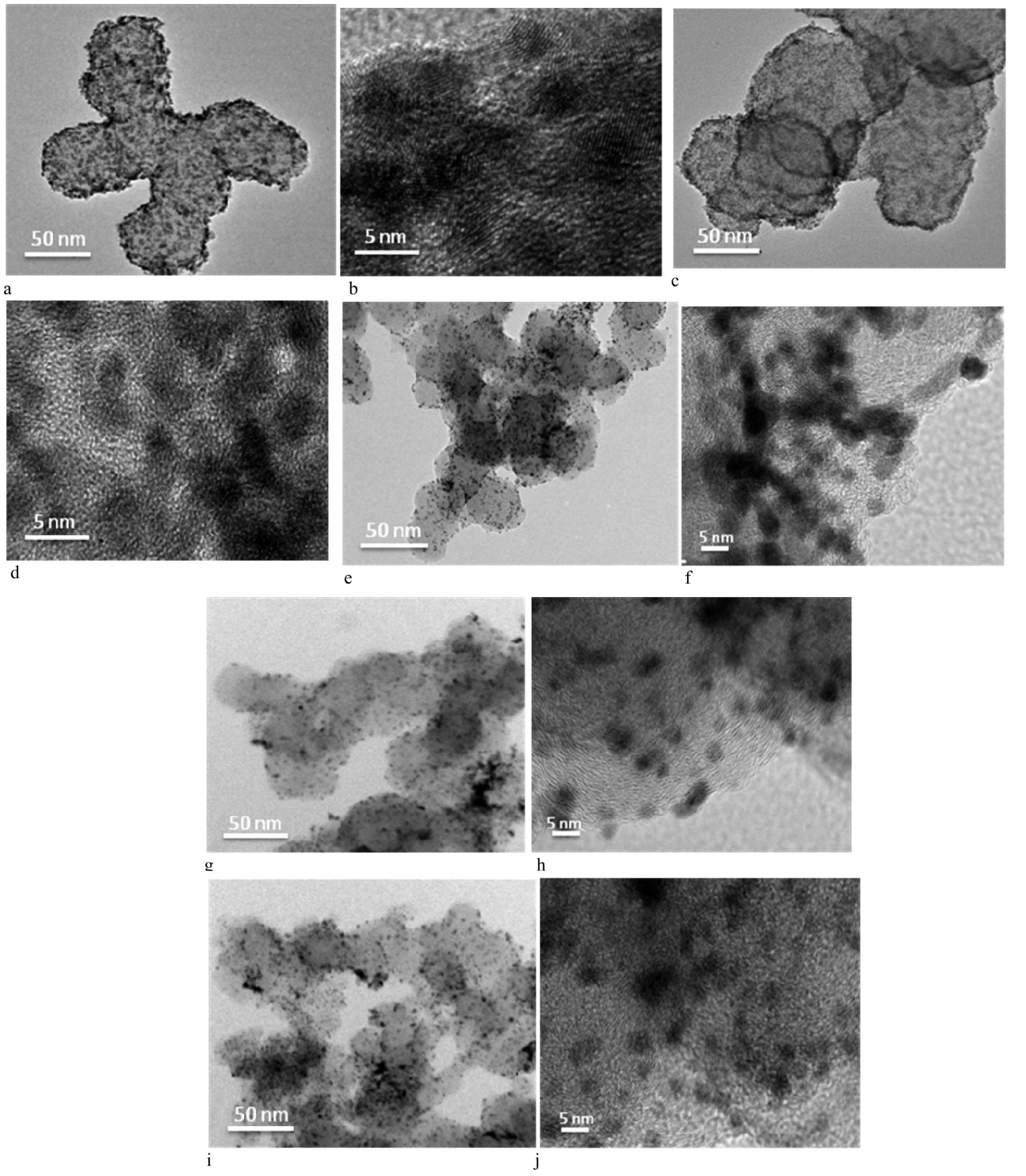

Figure 2. TEM images of (a, b) Pt/PCN, (c, d) Pt_1Ru_1/PCN, (e, f) Pt/C, (g, h) Pt_1Ru_1/C, and (i, j) Alfa Aesar PtRu/C.

diffraction of graphite carbon. The intensity of [002] peak is weak for Pt/PCN and PtRu/PCN catalysts, indicating a poorer graphite crystallinity of the samples PCNs. Several broad diffraction peaks could be indexed to the [111], [200], and [220] planes of a Pt face-centered cubic (fcc) crystal structure, suggesting an alloy formation based on the substitution of the Pt lattice sites. It was noted that with increasing proportion of Ru in the PtRu alloys, all diffraction peaks were shifted synchronously to higher 2θ values. The shift is an indication of the reduction in lattice constant. According to Vegard's law, lattice constant can be used as to measure the extent of alloying. In Figure 4, the lattice constant (a_o) for PtRu/PCN presents a decrease monotonically with the Ru content (3.925, 3.895, 3.888, and 3.879 Å for Pt/PCN, Pt_3Ru_1/PCN, Pt_2Ru_1/PCN, and Pt_1Ru_1/PCN catalysts, respectively). The reduction of a_o in PtRu/PCN arose primarily from the substitution of platinum atoms by Ru atoms, which led

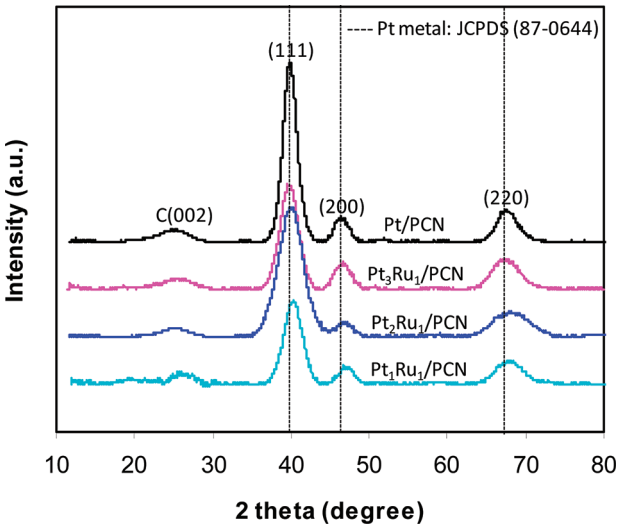

Figure 3. XRD patterns of PtRu/PCN catalysts.

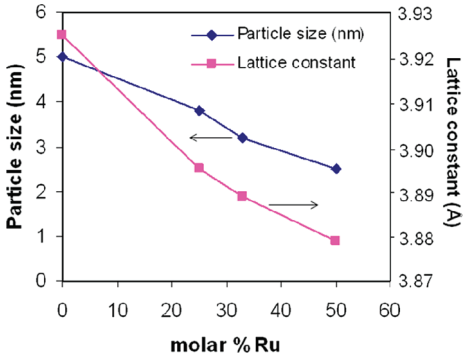

Figure 4. Dependence of particle size and lattice constant on the Ru content of PtRu/PCN catalysts.

to the contraction of the fcc lattice, an indication of the formation of PtRu alloys. The particle size was a volume-average calculated by the Scherrer equation

$$d\ (\text{Å}) = \frac{k\lambda}{\beta \cos\theta}$$

where k = coefficient (0.9), λ = wavelength of X-ray used (1.54056 Å), β = full width half maximum of respective diffraction peak (rad), and θ = angle at the position of peak maximum (rad).

The lattice constant contradiction also parallels to the trend of decreasing particle size with increasing Ru concentration. The particle size of PtRu alloy nanoparticles falls in the order Pt > Pt_3Ru_1 > Pt_2Ru_1 > Pt_1Ru_1, which can also be explained macroscopically by the incorporation of smaller Ru atoms into the Pt nanoparticle.

Electrochemical Performances. The electrochemical activities of the catalysts were tested by CV for MOR as the anodic half-cell reaction in DMFCs, and the corresponding CV curves of PtRu/PCN are shown in Figure 5a. There was significant feature (shape) difference between the CV curves of PtRu/PCN and of Pt/PCN as shown in Figure 5a. This indicates that the difference of CV curves between 0 and 0.2 V is not caused by PCN support.

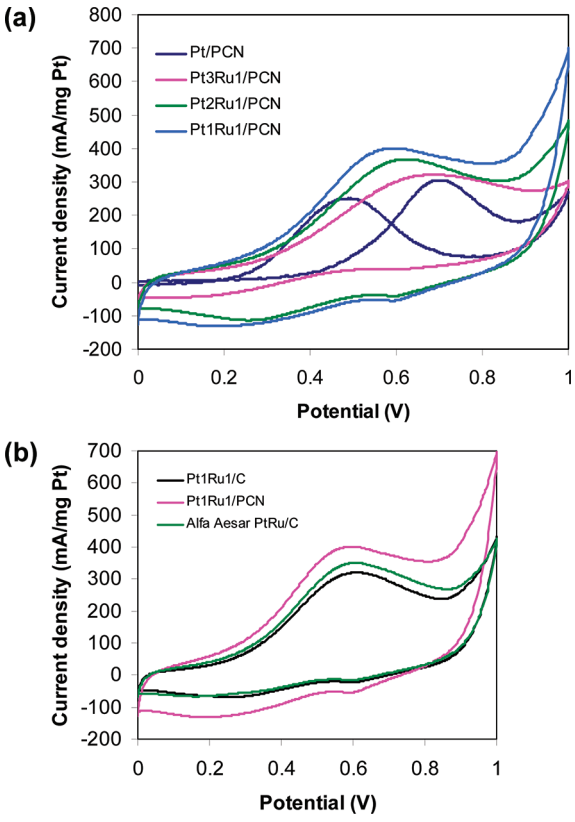

Figure 5. (a)Cyclic voltammograms of Pt/PCN and PtRu/PCN catalysts, and (b) Pt_1Ru_1/C, Pt_1Ru_1/PCN, and Alfa Aesar PtRu/C catalysts in 2M CH_3OH and 1M H_2SO_4 electrolyte at the scan rate of 50 mV s^{-1}.

The difference may be caused by PtRu. It can further be proven by Figure 5b, which are PtRu nanoparticles on different supports. In the forward scan, onset potential for MOR is about 0.2 V for Pt/PCN, 0−0.2 V may correspond to electrochemical double-layer (very small current). For three PtRu/PCN samples, the onset potential shifted negatively to 0.03 V. In the reverse scan, anodic peak at about 0.5 V for PtRu/PCN disappeared, cathodic current was maintained from about 0 to 0.7 V for PtRu/PCN. This means there is other reaction at 0−0.2 V except for electrochemical double-layer for PtRu/PCN. There was no significant feature difference for all PtRu/PCN catalysts. Anodic peaks appeared in both the forward and reverse (cathodic) scans for Pt/PCN catalyst. CO coverage starts at a potential of about 0.1 V. At more positive potentials the surface coverage by CO increases up to a maximum coverage, above which CO is gradually removed, and entirely removed by about 0.8 V.[32] The forward peak is caused by the removal of CO with adsorbing water and OH, followed by Pt−OH and Pt−O formation. Methanol molecules are not well oxidized on Pt−O surfaces. This is why the activity drops past the peak at high potentials. On the ensuing reverse sweep from 1 V there is no net CO accumulation on Pt and PtRu alloy. These surfaces are also very active for methanol electrooxidation.[32] The reverse sweep peak is caused by the desorption or reduction of the surface back to a metallic Pt surface on which the oxidation reaction happens very fast until at low potentials the surface becomes poisoned by CO-like species. Their mass catalytic activities in the forward scan (peak current density, which have been normalized to the Pt loading) of methanol oxidation decreased in the order Pt_1Ru_1>Pt_2Ru_1>Pt_3Ru_1. This can

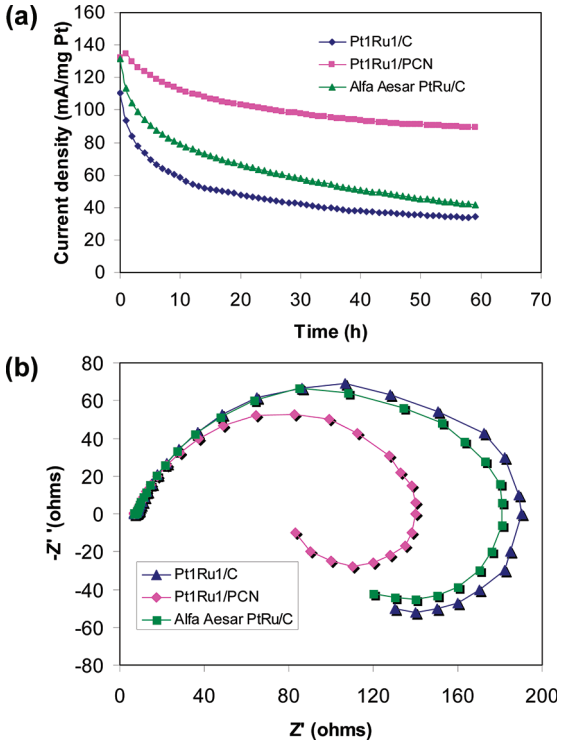

Figure 6. (a) Chronoamperometric measurements of catalysts at a constant potential of 0.4 V (vs. Ag/AgCl) in 2 M CH_3OH, 1 M H_2SO_4. (b) Impedance patterns of methanol electrooxidation on the catalysts in an Ar-saturated solution of 2 M CH_3OH and 1M H_2SO_4 at 0.4 V.

be attributed to the presence of Pt—Ru pair sites on the catalysts surface: Ru is known to adsorb oxygen-containing species (i.e., carbonaceous species) more favorably than pure Pt. The catalyst with the least carbonaceous accumulation, and hence most "tolerant" towards CO poisoning, was Pt_1Ru_1/PCN. The anodic peak potential was observed to shift cathodically with the increase in the ruthenium content of the alloy (from Pt_3Ru_1/PCN up to Pt_1Ru_1/PCN). The electrocatalytic activities of Pt_1Ru_1/C, Pt_1Ru_1/PCN and Alfa Aesar PtRu/C catalysts toward MOR are shown in Figure 5b. In the forward scan, although similar anodic peak potentials are observed for Pt_1Ru_1/C, Pt_1Ru_1/PCN and Alfa Aesar PtRu/C catayst, their peak current densities are 333, 420, and 380 mA/mg, respectively. The onset potentials at which the methanol oxidation initiates follow the order of Pt_1Ru_1/PCN< Alfa Aesar PtRu/C< Pt_1Ru_1/C. Pt_1Ru_1/PCN shows the highest mass activity and the lowest onset potential, which are desired for MOR. It was also found that after 700 cycles in Figure S5 (see the Supporting Information), activity of Pt_1Ru_1/PCN is still the highest even if substantially reduced to ~40% of its initial value, indicating its good stability for MOR comparable with the Alfa Aesar PtRu/C catalyst.

The stability of the catalysts was also examined through the steady-state chronoamperometry measurement in 2 M CH_3OH in 1 M H_2SO_4 at a constant potential of 0.4 V (vs. Ag/AgCl) as shown in Figure 6a. After a transient period, the current densities for the catalysts follow the order of Pt_1Ru_1/PCN > Alfa Aesar PtRu/C > Pt_1Ru_1/C. This is in agreement with the order of the catalytic activity obtained from the CV tests (Figure 5b). Pt_1Ru_1 nanoparticles supported on PCN showed a higher catalytic activity and more stable sustained current than on carbon black XC-72. Abundant N containing functionalities is crucial for improving the dispersion of PtRu alloy nanoparticles. PtRu nanoparticles are mainly distributed in micropores area.[6] The improved activity for methanol oxidation may be due to the higher surface area of the PCN for the catalyst dispersion. In addition, the significant catalytic enhancement associated with N-doped sample may also be attributed to intrinsic catalytic enhancement per unit of Pt surface area.[33] Further studies on the hydrogen desorption electrochemical surface area (ECSA) for PtRu/PCN and PtRu/C are ongoing to elucidate the origin of the catalytic enhancement of methanol oxidation for the PCN. The enhancement in catalytic performance may be attributed to the synergetic effects of the PCN support with abundant N containing functionalities, which improve the dispersion and immobilization of PtRu nanoparticles, and enhance intrinsic catalytic activity.

The EIS technique has been used to probe the interfacial processes and kinetics of electrode reactions in electrochemical systems. The methanol electro-oxidation on different catalysts at different potentials shows different impedance patterns for DMFC.[34−36] The Nyquist plots of the three catalysts are shown in Figure 6b. A typical pseudo-inductive behaviour was observed in the impedance plot, where a large arc at high frequency is accompanied by a small arc in the fourth quadrant at low frequency. An explanation for the occurrence of inductive behavior during methanol electrooxidation can be elucidated:[32] the active sites on Pt are covered initially with the CO_{ads} layer formed as one of the intermediates of methanol dehydrogenation, and thus deactivated at lower potentials. As potential increase, some of the weakly CO_{ads} begin to be oxidized, producing Pt active sites in the adsorbed CO layer. Subsequent methanol molecules then can be adsorbed in these active sites. Consequently, the reaction rate of methanol electrooxidation is sharply increasing. Namely, the so-called "pseudo-inductive" behavior results from the "relaxation phenomenon" between adsorption-dehydrogenation of methanol molecules and oxidation-adsorption of CO-like species. The smaller diameter of arc for Pt_1Ru_1/PCN at high frequency indicates the small charge-transfer resistance for MOR. The smaller intersect of impedance with real axis (Z') (designated as the polarization resistance) at low frequency for Pt_1Ru_1/PCN compared with Alfa Aesar PtRu/C and Pt_1Ru_1/C suggests the faster overall MOR rate, namely, dehydrogenation of methanol molecules and oxidation of intermediate CO_{ads} species.[34,35] EIS observation is consistent with the results in Figures 5b and 6a, further confirming the enhanced electrocatalytic activity of the Pt_1Ru_1/PCN catalyst.

CONCLUSION

PCNs with 0.05 of the N/C atomic ratio were prepared by chemical activation of nonporous carbon nanospheres (CNs) that were obtained via carbonizing polypyrrole nanospheres (PNs). The catalysts, Pt and PtRu nanoparticles supported on PCNs and Vulcan XC-72 carbon, were successfully synthesized by a simple microwave-assisted polyol procedure. Uniform and well-dispersed Pt and PtRu particles with narrow particle size distribution on PCNs were observed. The alloy catalyst (Pt_1Ru_1/PCN) showed the highest catalytic activity and better CO tolerance than the other PtRu and Pt-only catalysts. Compared to commercial Alfa Aesar PtRu catalyst, Pt_1Ru_1/PCN reveals an enhanced and durable catalytic activity in methanol oxidation. The improved activity for methanol oxidation may be attributed to the synergetic effects of the PCN support with abundant N containing functionalities, which improve the dispersion and

immobilization of PtRu nanoparticles, and intrinsic catalytic activity enhancement.

■ ASSOCIATED CONTENT

Supporting Information. TEM images of PNs (a), CNs (b), and PCNs (c), and high-magnification TEM images of CNs (d) and PCNs (e); N_2 adsorption-desorption isotherms and pore size distribution (PSD) of Vulcan carbon; TEM images of Pt_3Ru_1/PCN (a, b) and Pt_2Ru_1/PCN (c, d); TG curves of (a) Pt/PCN, Pt_1Ru_1/PCN and Alfa Aesar PtRu/C, and (b) PCNs and Vulcan carbon; CV curves of catalysts Pt/PCN (a), Pt_1Ru_1/PCN (b) and Alfa Aesar PtRu/C(c). This material is available free of charge via the Internet at http://pubs.acs.org.

■ AUTHOR INFORMATION

Corresponding Author

*Tel: +65-68727532 (Z.L.). E-mail: zl-liu@imre.a-star.edu.sg (Z. L.).

■ ACKNOWLEDGMENT

The authors are grateful to the IMRE of A*STAR for financial support. Dr. F. Su is grateful to the Chinese Academy of Sciences (Hundred Talents Program) and National Natural Science Foundation of China (21031005) for financial support.

■ REFERENCES

(1) Vigier, F.; Rousseau, S.; Coutanceau, C.; Leger, J. M.; Lamy, C. *Top. Catal.* **2006**, *40*, 111.
(2) Dicks, A. L. *J. Power Sources* **2006**, *156*, 128.
(3) Wen, Z.; Wang, Q.; Li, J. *Adv. Funct. Mater.* **2008**, *18*, 959.
(4) Stein, A.; Wang, Z.; Fierke, M. A. *Adv. Mater.* **2009**, *21*, 265.
(5) McCreery, R. L. *Chem. Rev.* **2008**, *108*, 2646.
(6) Yu, J. S.; Kang, S.; Yoon, S. B.; Chai, G. S. *J. Am. Chem. Soc.* **2002**, *124*, 9382.
(7) Chai, G. S.; Yoon, S. B.; Yu, J. S.; Choi, J. H.; Sung, Y. E. *J. Phys. Chem. B* **2004**, *108*, 7074.
(8) Liu, S. H.; Yu, W. Y.; Chen, C. H.; Lo, A. Y.; Hwang, B. J.; Chien, S. H.; Liu, S. B. *Mater. Chem.* **2008**, *20*, 1622.
(9) Wang, Y.; Wang, X.; Li, C. M. *Appl. Catal. B* **2010**, *99*, 229.
(10) Shao, Y.; Sui, J.; Yin, G.; Gao, Y. *Appl. Catal. B* **2008**, *79*, 89.
(11) Ma, Y.; Jiang, S.; Jian, G.; Tao, H.; Yu, L.; Wang, X.; Wang, X.; Zhu, J.; Hu, Z.; Chen, Y. *Energy Environ. Sci.* **2009**, *2*, 224.
(12) Kim, M.; Hwang, S.; Yu, J. -S. *J. Mater. Chem.* **2007**, *17*, 1656.
(13) Di Noto, V.; Negro, E.; Gliubizzi, R.; Lavina, S.; Pace, G.; Gross, S.; Maccato, C. *Adv. Funct. Mater.* **2007**, *17*, 3626.
(14) Yue, B.; Ma, Y.; Tao, H.; Yu, L.; Jian, G.; Wang, X.; Wang, X.; Lu, Y.; Hu, Z. *J. Mater. Chem.* **2008**, *18*, 1747.
(15) Lei, Z.; An, L.; Dang, L.; Zhao, M.; Shi, J.; Bai, S.; Cao, Y. *Microporous Mesoporous Mater.* **2009**, *119*, 30.
(16) Liu, H.; Shi, Z.; Zhang, J.; Zhang, L.; Zhang, J. *J. Mater. Chem.* **2009**, *19*, 468.
(17) Su, F.; Zhou, Z.; Guo, W.; Liu, J.; Tian, X. N.; Zhao, X. S. In *Chem. Phys. Carbon*; Radovic, L. R., Ed.; Marcel Dekker: New York, 2008; Vol. 30, pp 63−128.
(18) Stein, A.; Wang, Z.; Fierke, M. A. *Adv. Mater.* **2009**, *21*, 265.
(19) Lei, Z.; Zhao, M.; Dang, L.; An, L.; Lu, M.; Lo, A. Y.; Yu, N.; Liu, S. B. *J. Mater. Chem.* **2009**, *19*, 5985.
(20) Choi, B.; Yoon, H.; Park, I. S.; Jang, J.; Sung, Y. E. *Carbon* **2007**, *45*, 2496.
(21) Wu, J; Hu, F; Shen, P. K.; Li, C. M.; Wei, Z. *Fuel Cells* **2010**, *10*, 106.
(22) Su, F.; Tian, Z.; Poh, C. K.; Wang, Z.; Lim, S. H.; Liu, Z. L.; Lin, J. *Chem. Mater.* **2010**, *22*, 832.
(23) Wang, Y.; Su, F.; Wood, C. D.; Lee, J. Y.; Zhao, X. S. *Ind. Eng. Chem. Res.* **2008**, *47*, 2294.
(24) Liu, Z.; Lee, J. Y.; Chen, W.; Han, M.; Gan, L. M. *Langmuir* **2004**, *20*, 181.
(25) Cheng, F.; Liang, J.; Zhao, J.; Tao, Z. J.; Chen *Chem. Mater.* **2008**, *20*, 1889.
(26) Jaroniec, M.; Choma, J.; Gorka, J.; Zawislak, A. *Chem. Mater.* **2008**, *20*, 1069.
(27) Wang, J. N.; Zhang, L.; Niu, J. J.; Yu, F.; Sheng, Z. M.; Zhao, Y. Z.; Chang, H.; Pak, C. *Chem. Mater.* **2007**, *19*, 453.
(28) Chen, J.; Wang, M.; Liu, B.; Fan, Z.; Cui, K.; Kuang, Y. *J. Phys. Chem. B* **2006**, *110*, 11775.
(29) Yang, D.; Sacher, E. *Chem. Mater.* **2006**, *18*, 1811.
(30) Zhang, G.; Yang, D.; Sacher, E. *J. Phys. Chem. C* **2007**, *111*, 565.
(31) Yang, D.; Sacher, E. *J. Phys. Chem. C* **2008**, *112*, 4075.
(32) Markovic, N. M.; Gasteiger, H. A.; Ross, P. N.; Jiang, X.; Villegas, I.; Weaver, M. J. *Electrochim. Acta* **1995**, *40*, 91.
(33) Zhou, Y.; Pasquarelli, R.; Holme, T.; Berry, J.; Ginley, D.; O'Hayre, R. *J. Mater. Chem.* **2009**, *19*, 7830.
(34) Hsing, I. M.; Wang, X.; Leng, Y. J. *J. Electrochem. Soc.* **2002**, *149*, A615.
(35) Chakraborty, D.; Chorkendorff, I.; Johannessen, T. *J. Power Sources* **2006**, *162*, 1010.
(36) Wang, Z. B.; Yin, G. P.; Shao, Y. Y.; Yang, B. Q.; Shi, P. F.; Feng, P. X. *J. Power Sources* **2007**, *165*, 9.